

Dalton Transactions

An international journal of inorganic chemistry

Accepted Manuscript

This article can be cited before page numbers have been issued, to do this please use: S. Sun, X. Jiang, Z. Wang, H. Lei, Y. Zhai and P. Wang, *Dalton Trans.*, 2025, DOI: 10.1039/D5DT01534K.



This is an Accepted Manuscript, which has been through the Royal Society of Chemistry peer review process and has been accepted for publication.

Accepted Manuscripts are published online shortly after acceptance, before technical editing, formatting and proof reading. Using this free service, authors can make their results available to the community, in citable form, before we publish the edited article. We will replace this Accepted Manuscript with the edited and formatted Advance Article as soon as it is available.

You can find more information about Accepted Manuscripts in the [Information for Authors](#).

Please note that technical editing may introduce minor changes to the text and/or graphics, which may alter content. The journal's standard [Terms & Conditions](#) and the [Ethical guidelines](#) still apply. In no event shall the Royal Society of Chemistry be held responsible for any errors or omissions in this Accepted Manuscript or any consequences arising from the use of any information it contains.

Prussian blue analogues for high-performance sodium ion battery cathodes: recent advances and challenges

Shumin Sun,^{*a} Xingqi Jiang,^a Ziyu Wang,^a Haibo Lei,^a Yongqin Zhai,^a and Peiyuan Wang^{*ab}

Received 00th January 20xx,
Accepted 00th January 20xx

DOI: 10.1039/x0xx00000x

Prussian blue analogues (PBAs) have gained considerable attention as promising cathode materials for sodium-ion batteries (SIBs) due to their three-dimensional open framework structure, cost-effectiveness, and high theoretical capacity. Currently, the fundamental research and commercial exploration of PBAs in SIBs are making robust progress. This review summarizes the recent advance and mainly highlight five key developments: (1) innovative synthesis methods, (2) compositional engineering, (3) advanced structural designs, (4) post-treatment and remediation techniques and (5) scalable synthesis. Finally, we present a forward-looking perspective on future research directions, emphasizing the importance of multidisciplinary approaches combining advanced characterization techniques, and systematic engineering optimization to facilitate their commercialization for energy storage systems.

Introduction

Sodium-ion batteries (SIBs) have emerged as a promising alternative to lithium-ion batteries (LIBs) for energy storage system, owing to sodium's natural abundance and cost advantages. Their performance largely depends on cathode materials, such as energy density, cost efficiency, cycling stability, and safety. Current research on SIBs cathodes primarily concentrates on four categories: layered transition metal oxides,^{1, 2} polyanionic compounds,³ Prussian blue analogues (PBAs),^{4, 5} and organic compounds.⁶ Layered transition metal oxides, such as Na_xCoO_2 ,^{7, 8} NaFeO_2 ,^{9, 10} NaMnO_2 ,¹¹ NaCrO_2 ,¹² and $\text{NaNi}_{1/3}\text{Fe}_{1/3}\text{Mn}_{1/3}\text{O}_2$,^{13, 14} exhibit high specific capacities over 200 mAh g⁻¹, while they universally suffer from structural instability caused by complicated phase transitions during sodium (de)intercalation. Polyanionic compounds comprise phosphates (e.g., NaFePO_4 , $\text{Na}_3\text{V}_2(\text{PO}_4)_3$), pyrophosphates ($\text{Na}_2\text{MP}_2\text{O}_7$), fluorophosphates ($\text{Na}_2\text{MPO}_4\text{F}$), and sulfates ($\text{Na}_2\text{Fe}_2(\text{SO}_4)_3$). Despite their structure stability and long cycle lifetime, low theoretical capacity (120 mAh g⁻¹) will throughout restrict their future applications. Most organic compounds have low electronic conductivity and are easily soluble in organic electrolytes, which poses great challenges to their rate performance and cycling stability in practical applications. PBAs stand out due to their robust 3D open framework, high theoretical capacity (170 mAh g⁻¹), and low-cost synthesis routes.^{4, 5}

PBAs are a great family of metal–organic frameworks, and their chemical formulas could be represented as

$\text{A}_x\text{M}_1[\text{M}_2(\text{CN})_6]_y\Box_{1-y} \cdot z\text{H}_2\text{O}$. Here, M_1 represents the transition metal ions in a high-spin state (M_{HS}) coordinated to N atom, while M_2 refers a transition metal in a low-spin state (M_{LS}) bonded to C atoms of the CN ligands, respectively. Typical PBAs are usually face-centered cubic (FCC) lattice structure (space group: $Fm\bar{3}m$), where metal sites M_1 and M_2 occupy the vertex positions and are interconnected via cyanide bridging ligands aligned along the cube edges. The crystal structure exhibits polymorphic transformations among cubic, monoclinic, rhombohedral, and tetragonal phases, governed by Na^+ concentration, water content, and transition metal (Fig. 1).^{15, 16} Among the PBAs, metal hexacyanoferrates (M-HCFs , $\text{M}=\text{Fe}, \text{Mn}, \text{Co}, \text{Ni}, \text{Cu}, \text{Zn}$ etc.), formulated as $\text{A}_x\text{M}[\text{Fe}(\text{CN})_6]_y\Box_{1-y} \cdot z\text{H}_2\text{O}$, have garnered considerable interest due to their high theoretical

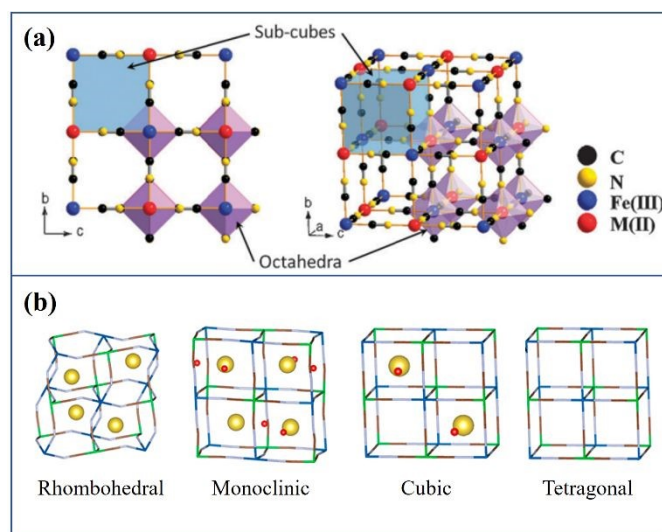


Fig. 1 Framework of PBAs (a). Reproduced with permission. Copyright 2012, Royal Society of Chemistry.¹⁵ Crystal structure of PBAs (b). Reproduced with permission. Copyright 2015, American Chemical Society.¹⁶

^a College of Material and Chemical Engineering, Zhengzhou University of Light Industry, Zhengzhou 450001, P. R. China. E-mail: smsun@zzuli.edu.cn.

^b Henan Provincial Key Laboratory of Surface and Interface Science, Zhengzhou University of Light Industry, Zhengzhou 450001, P. R. China. E-mail: peiyuanwang@zzuli.edu.cn

capacity and cost-effectiveness.^{17–20} The following discussion will focus on this category of compounds.

The pioneering work by Goodenough's group in 2012 demonstrated the electrochemical potential of PBAs ($\text{KMFe}(\text{CN})_6$, $\text{M} = \text{Fe, Co, Ni, Mn, Zn}$) for SIBs, marking the beginning of extensive research in this field.¹⁵ Traditional co-precipitation methods often yield PBAs with high $\text{Fe}(\text{CN})_6$ vacancy and water content, leading to structural instability. To mitigate this, Huang's group and Yang's group separately reported the citrate-assisted co-precipitation method, producing low-defect PBAs with superior cycling stability and capacity.^{21, 22} In 2014, You et al. developed a single iron-source precursor method to synthesize high-quality $\text{Na}_{0.61}\text{Fe}[\text{Fe}(\text{CN})_6]_{0.94}$ with minimal vacancies and water content.²³ In order to address the challenge of Na^+ deficiency in PBAs, reductant and inert N_2 atmosphere were further introduced, which effectively suppressed Fe^{2+} oxidation and obtained Na-rich $\text{Na}_{1.63}\text{Fe}[\text{Fe}(\text{CN})_6]_{0.89}$ with enhanced electrochemical performance.²⁴ In 2019, Gong et al. adopted a facile ball-milling method to synthesize the Fe-MnPBA without additional additives.²⁵ The particles of Fe-MnPBA can be downsized to ~ 50 nm and the ultrafine particles favor the fast Na^+ diffusion.

The electrochemical behavior of PBAs is predominantly determined by their composition and structural characteristics. PBAs store sodium ions through reversible redox reactions of transition metals. Dual-electron transfer PBAs (DE-PBAs; $\text{M} = \text{Mn, Fe, Co}$) exhibit two-step redox activity at both M- and Fe-sites, delivering high theoretical capacities (~ 170 mAh g^{-1}), but suffering from structural degradation due to phase transitions. In contrast, single-electron transfer PBAs (SE-PBAs; $\text{M} = \text{Zn, Ni, Cu}$) restrict redox activity to Fe-sites, achieving lower capacities (~ 85 mAh g^{-1}) but superior cyclability (>2000 cycles) owing to their robust frameworks.^{23, 24} The intrinsic $[\text{Fe}(\text{CN})_6]$ vacancies and crystal water in PBAs also significantly influence their electrochemical performance and stability. The $[\text{Fe}(\text{CN})_6]$ vacancies introduce lattice defects, impede charge transfer kinetics, and reduce available Na^+ storage sites. The liberation of the crystal water during battery operation poses significant safety concerns, as their migration into the electrolyte triggers deleterious side reactions accompanied by gaseous byproducts.²⁶

Therefore, the commercialization of PBAs as cathodes for SIBs faces multiple crucial challenges: (1) Intrinsic $[\text{Fe}(\text{CN})_6]$ vacancies and crystal water significantly reduce available sodium storage sites and may compromise structural stability, (2) Irreversible phase transitions during electrochemical cycling cause progressive structural degradation and capacity fading, and (3) Scalable synthesis methods must be developed to enable cost-effective mass production.¹⁹ In order to address these issues, researchers optimized the synthesis method, adjust the composition and structure, etc. So far, the significant progresses of PBAs have been achieved, this review mainly focuses on the recent progress of PBAs cathode materials for SIB applications, including advanced synthesis methods, post-treatment techniques, composition engineering, morphology control, and scalable synthesis, highlighting their impact on the

electrochemical performance. Finally, we present a forward-looking perspective on future research directions to facilitate their commercialization for grid-scale energy storage systems.

Recent progress in improving the electrochemical performance of PBAs

optimized synthesis strategy

PBAs are typically synthesized through complexing-agent assisted co-precipitation, hydrothermal, or electrodeposition methods. The hydrothermal method usually involves the usage of $\text{Na}_4\text{Fe}(\text{CN})_6$ solution as a single iron-source under hydrochloric acid (HCl) addition at high temperatures. The Fe^{2+} ion can be slowly dissociated to react with residual $[\text{Fe}(\text{CN})_6]^{4-}$ ion. In this way, Fe-HCF with low $[\text{Fe}(\text{CN})_6]$ vacancies and water can be obtained, while the yield is very low. To achieve high-yielding Fe-HCF, Wang et al. developed an efficient method employing an acetic acid-sodium acetate (HAc-NaAc) buffer system as a replacement for the diluted HCl.²⁷ This buffer system provides stable, low-concentration H^+ ions to enable controlled decomposition of $[\text{Fe}(\text{CN})_6]^{4-}$, resulting in highly crystalline, sodium-rich Fe-HCF ($\text{Na}_{1.88}\text{Fe}[\text{Fe}(\text{CN})_6]_{0.97} \cdot 2.06\text{H}_2\text{O}$) with 95% yield - a significant improvement over the 15% yield obtained using the dilute HCl solution.

Tang et al. developed an epitaxial nucleation-assisted crystallization strategy to suppress structural defects in NaFeHCF.²⁸ Utilizing graphene oxide (GO) as an epitaxial growth platform—enabled by its minimal lattice misfit (4.87%) with NaFeHCF and electronegative functional groups ($-\text{COOH}$, $-\text{OH}$, $-\text{CH}(\text{O})\text{CH}-$)—this approach yielded uniquely truncated cubic nanocrystals with drastically reduced defect density (0.08 per formula unit). The enhanced lattice regularity accelerated Na^+ diffusion fivefold, achieving unprecedented rate performance (Fig. 2a).

PBAs are mostly prepared in aqueous solution, water molecular inevitably inserts into the framework of PBAs due to the presence of $[\text{Fe}(\text{CN})_6]$ vacancies. In order to control water and defect formation in PBAs, solvent engineering approaches is an effective way. Geng et al. developed a microwave-assisted solvothermal approach to prepare high-quality NaFeHCF nanoparticles using anhydrous ethanol as the reaction solvent.²⁹ The tuned NaFeHCF exhibited low water content as well as good thermal stability. It delivers a high initial discharge capacity of 150 mAh g^{-1} , good rate capability and cycling life over 500 cycles. Xu et al. proposed a facile "ligand pre-exchange strategy" to synthesize highly crystallized PBAs (Fig. 2b).³⁰ Ethylene glycol (EG) was introduced to exchange with H_2O in $[\text{Fe}(\text{H}_2\text{O})_6]^{2+}$ to form a water-deficient solvated structure of $[\text{Fe}(\text{H}_2\text{O})_x(\text{EG})_{(6-x)}]^{2+}$, which resulted in a reduction of the amount of coordinated water and vacancy defects in the PBAs. The PB-EG-5 electrode prepared by this strategy exhibited excellent sodium storage performance and fast kinetics, with a specific capacity of 91.3 mA h g^{-1} at 1000 mA g^{-1} in a half-cell and capacity retention of 70% after 1000 cycles. Li et al. introduced a synergistic approach of PBAs combining non-aqueous phase precursor synthesis and controlled water-

concentration secondary crystallization.³¹ The process involves preparing a PB precursor in a glycerol system, followed by secondary crystallization in a water/ethanol-mixed solvent with a precisely regulated water content, achieving the dual objectives of water content reduction and crystal morphology optimization. The optimized PB50-24 material exhibited a highly regular cubic morphology with a remarkably low interstitial water content of 2.1%. Electrochemical tests demonstrated outstanding performance—an initial charge–discharge capacity of 120 mAh g⁻¹ at 1C rate, the retention of 105 mAh g⁻¹ after 100 cycles, and a high rate capability of 86 mAh g⁻¹ at 10C, representing significant improvements in cycling stability and rate performance.

Ball milling solid-state synthesis has also emerged as an effective method for preparing PBAs with low water content.^{25, 32, 33} For instance, Peng et al. developed a "water-in-salt" nanoreactor strategy to synthesize highly crystalline Na_{2-x}MnFe(CN)₆ with minimal defects and water.³² The resulting MnHCF-S-170 particles exhibit a uniform ellipsoidal morphology (~30 nm) and a chemical composition of Na_{1.66}Mn[Fe(CN)₆]_{1.00}·1.90H₂O. The reduced Fe(CN)₆ vacancies enhance structural integrity, facilitating robust Na-ion transport channels and fast migration kinetics. Additionally, the low

interstitial water content minimizes electrode-electrolyte side reactions, improving electrochemical performance. Gao et al. introduced a solvent-free, zero-waste mechanochemical approach for large-scale production of NFS@Fe-PB, a composite comprising cubic PBA (c-NFFHCF) and monoclinic sulfate (m-NFS), with the formula Na_{3.9}Fe₂[Fe(CN)₆]_{0.98}(SO₄)_{1.99}·0.72H₂O (Fig. 2c).³³ This material demonstrates high crystallinity and stable performance across a broad temperature range (-10 to 50 °C), delivering a specific capacity of 94 mAh g⁻¹ at 10 mA g⁻¹ and retaining 82.15% capacity after 500 cycles. The m-NFS phase stabilizes the structure by mitigating distortion in c-NFFHCF during cycling, and the synergistic effects between the two phases enable rapid Na-ion storage and structural reversibility.

Advanced post-treatment and remediation technique

PBAs with high sodium content, low defect concentration, and minimal crystal water are considered ideal cathode materials for SIBs. In addition to optimized synthesis methods, advanced post-treatment processes are equally critical. Washing and purifying the as-prepared sample is an important process, while washing the PBAs with water results in Na⁺ loss and Fe²⁺ oxidation. To address this challenge, Wang et al. developed an innovative washing strategy using a reducing sodium ascorbate aqueous solution, effectively suppressing these undesirable Na⁺ loss and Fe²⁺ oxidation.³⁴ The prepared PW-H (Na_{1.88}Fe[Fe(CN)₆]_{0.84}·3.11H₂O) exhibited higher sodium content and fewer vacancies compared to conventionally water-washed samples (PW-L, Na_{1.56}Fe[Fe(CN)₆]_{0.83}·3.41H₂O). When evaluated as a cathode in SIBs, PW-H delivered a specific capacity of 140 mAh g⁻¹ at 0.1 C with excellent cycling stability (Fig. 3a-c).

The removal of crystalline water from PBAs is typically achieved through controlled thermal treatment. Pioneering work by Song et al. demonstrated that vacuum drying at 100°C effectively eliminates interstitial water from Na₂₋₆MnHCF.¹⁶ Maddar et al. provided a deeper insight into the dehydration kinetics of Prussian White cathode materials, establishing that water removal follows temperature- and atmosphere-dependent kinetics.³⁵ Recently Xing et al. removed 90.1 wt % of the crystal water in Fe-PB by drying at 130 °C under vacuum for 12 h, and the dehydrated Fe-PB maintained 85.5% of its initial capacity after 1200 cycles at 300 mA g⁻¹.³⁶

However, a significant challenge remains as heat-treated materials readily reabsorb water when exposed to ambient air. So, electrolyte modification has emerged as a practical solution to mitigate water-related issues. Wang et al. demonstrated that adding 1wt% (3-aminopropyl)triethoxysilane (APTS) to conventional electrolyte effectively minimizes interfacial side reactions.³⁷ This additive captures harmful water molecules, thereby protecting Fe-based PBAs from HF-induced damage and significantly enhancing cycle life (Fig. 3d-f). Remarkably, the material maintained a capacity of 59.2 mAh g⁻¹ after 12,000 cycles at 1.0 A g⁻¹. An alternative approach was developed by Du et al. through the design of a sodium polyacrylate "water-absorbing layer" (Fig. 3g-i).³⁸ This functional layer selectively captures water released from PBAs during cycling while forming

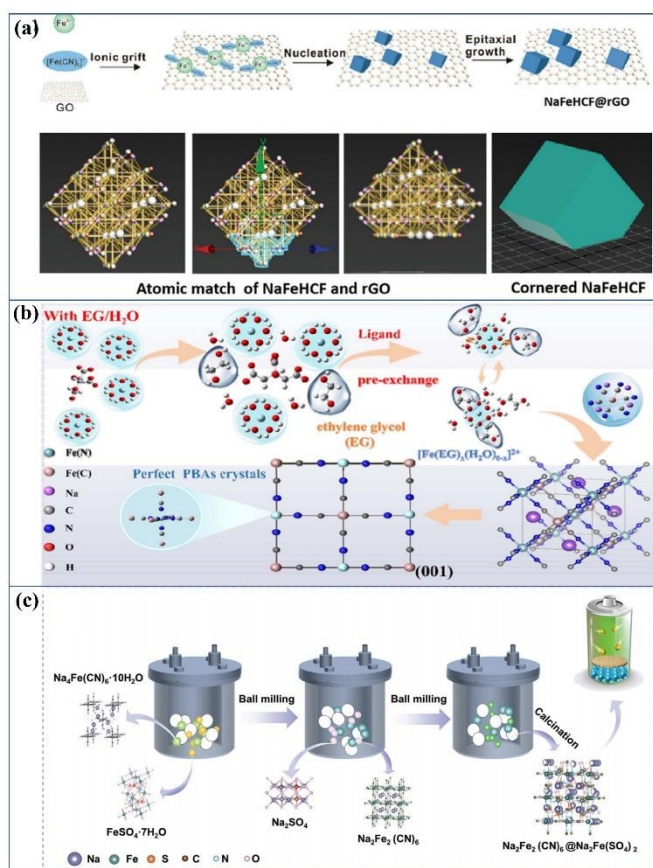


Fig. 2 Schematic illustration of NaFeHCF@rGO synthesis structural diagrams of cubic and cornered NaFeHCF (a). Reproduced with permission. Copyright 2024, Wiley.²⁸ Schematic of the synthesis of PB-EGs via the ligand pre-exchange strategy (b). Reproduced with permission. Copyright 2025, Royal Society of Chemistry.³⁰ Schematic illustration of the synthesis of NFS@Fe-PB sample based on mechanochemical ball milling strategy (c). Reproduced with permission. Copyright 2025, Wiley.³³

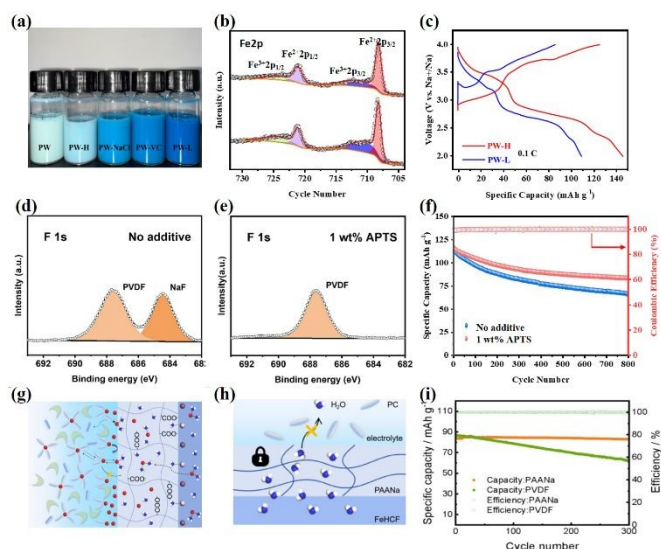


Fig. 3 Digital photographs (a), XPS spectra (b), the first charge and discharge curves (c) of PW-H and PW-L of the synthesized PBAs. Reproduced with permission. Copyright 2022, Royal Society of Chemistry.³⁴ XPS spectra of F 1s for the cycled cathodes in both the electrolyte without the additive (d) with 1 wt % APTS additive electrolyte (e) and cycling performance of NiMnFe-PBA with 1 wt% APTS additive and no additive at 200mA g⁻¹ (f). Reproduced with permission. Copyright 2025, Elsevier.³⁷ Sodium ion solvation/desolvation and transport behavior upon selective asymmetric polarization of the PAANA "diaper" interface layer during the charge/discharge cycle when encountering moisture (g), Water molecules are captured by the PAANA "diaper" (h), and Electrochemical cycling performance of the PAANA and PVDF electrodes at 150 mA g⁻¹ (i). Reproduced with permission. Copyright 2025, Elsevier.³⁸

an asymmetric interfacial layer through ionization. This dual mechanism enhances both interfacial kinetics and structural stability, enabling 97.9% capacity retention after 300 cycles at 0.15 A g⁻¹.

The rapid crystallization process of PBAs generates numerous Fe(CN)₆ vacancies, which compromise structural integrity and induce capacity fading due to structural degradation during prolonged electrochemical cycling. In the aqueous synthesis of FeHCF, high spin Fe²⁺ (HS-Fe²⁺) cations in the vacancies are exposed to H₂O, OH⁻, and [Fe(CN)₆]⁴⁻ anions. DFT calculations show that the binding energy between HS-Fe²⁺ and [Fe(CN)₆]⁴⁻ is the lowest, which indicates that HS-Fe²⁺ cations in the vacancies are more likely to coordinate with the [Fe(CN)₆]⁴⁻ anions. Based on DFT calculations, Wan et al. proposed a post-synthetic vacancy repairing strategies by adding the prepared vacancy-rich FeHCF to a highly concentrated Na₄Fe(CN)₆ solution (0.8 mol L⁻¹).³⁹ The vacancy defects could be significantly reduced by ~26% after post-synthetic vacancy repairing. Vacancy-repaired FeHCF-P cathodes significantly reduce electrolyte decomposition at the cathode-electrolyte interface and suppress the dissolution of Fe ions during the charge–discharge process, as confirmed by electrochemical analysis. Thus, the vacancy repairing strategy in a concentrated [Fe(CN)₆]⁴⁻ solution could effectively reinforce the crystalline structure of FeHCF and guarantee excellent cycling stability.

Compositional engineering

Despite significant efforts to minimize water content in PBAs through optimized synthesis and thermal treatment, achieving stable, low-water frameworks remains challenging. So

researchers adopted composition engineering to reduce the water content.^{40–42} For instance, Gao et al. used larger K⁺ (1.33 Å) to substitute Na⁺ (1.02 Å) in Na_{2-x}FeMn[Fe(CN)₆] (FeMnPBA), finding that K⁺ doping reduces interstitial H₂O occupancy and expands ion migration channels; the optimal 3% K-doped material achieved a water content of 6.9%, delivering 139.1 mAh g⁻¹ at 100 mA g⁻¹ and retaining 77.1% capacity after 700 cycles (Fig. 4a).⁴¹ Similarly, Xu et al. introduced K⁺ into MnFe-PBAs, creating a mixed Na/K phase (Na_{1.08}K_{0.74}Mn[Fe(CN)₆]_{0.86}□_{0.14}·1.86H₂O, NaKMhCF) with reduced water/vacancies compared to pure Na phases, which delivered 129.3 mAh g⁻¹ at 10 mA g⁻¹ alongside excellent rate capability and cycling stability.⁴² Alternatively, Li et al. employed an ion-exchange method to synthesize low-water K/Na mixed iron hexacyanoferrate (KNaFeHCF); their optimal sample (KNaFeHCF-12h) reduced water content by 21.2% compared to co-precipitated NaFeHCF and exhibited excellent electrochemical performance, with capacities of 130.33 mAh g⁻¹ at 0.1 C and 99.49 mAh g⁻¹ at 30 C.⁴⁰ It can be concluded that K-doping strategy can minimize the water content in PBAs.

Fe- and Mn-based PBAs (Fe-HCF and Mn-HCF) are promising cathode materials for SIBs, offering high theoretical capacities and cost-effectiveness. However, their practical application is hindered by irreversible phase transitions and poor cycling stability, particularly the Mn³⁺-induced Jahn-Teller distortion in Mn-HCF. To address these limitations, metal substitution has emerged as an effective strategy.^{43, 44} Recently, Li et al. employed the integrated crystal orbital Hamilton population (ICOHP) function to evaluate N-transition metal (N-TM) bond strengths, identifying Cu–N as the most stable due to its lowest ICOHP value, which indicates that Cu doping can improve the stability of PBAs compared to other dopants (Fig. 4b–c).⁴⁵

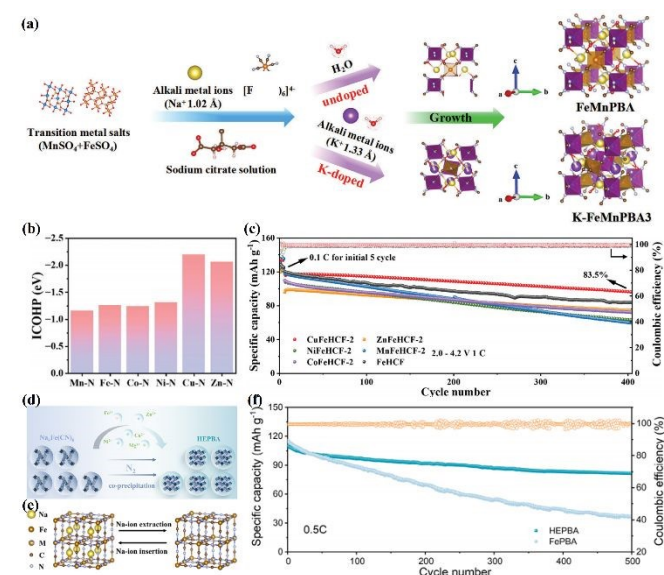


Fig. 4 Schematic illustration of the synthesis process of FeMnPBA and K-FeMnPBA3 (a). Reproduced with permission. Copyright 2024, Wiley.⁴¹ The ICOHP values of various TM-N bonds (b), Cycling performance of TMFeHCF-2 samples at a current density of 1 C (c). Reproduced with permission. Copyright 2024, Wiley.⁴⁵ Schematic representation of the HEPBA (d), Illustration of sodium storage mechanism for HEPBA (e) and Cycling performance of HEPBA and FeHCF at 0.5C (f). Reproduced with permission. Copyright 2025, Wiley.⁴⁹

Experimental validation confirmed that Cu-doped Fe-HCF (CuFeHCF-2) delivered superior cyclability (83.5% capacity retention after 400 cycles at 1 C), supported by in situ XRD revealing a reversible monoclinic-cubic transition. Zhang et al. introduced Zn into Fe-HCF via ion exchange, achieving minimal lattice distortion ($\sim 3.6\%$ volume change) and a stable cubic-tetragonal transition, significantly enhancing cycling stability.⁴⁶ Ni/Mn-doped Fe-HCF reported by Wang et al. displayed the specific capacity 122.8 mAh g^{-1} at a current density of 10 mA g^{-1} , and exhibited a significant improvement in both the mid-value voltage and cycling stability.³⁷ Ternary PBAs (T-PBA) with Cu/Fe co-doping in Mn-HCF exhibited a solid-solution reaction mechanism, consistently maintain a cubic phase with smaller lattice distortion rather than occur in conventional three-phase transition during the charging and discharging processes, forcefully inhibiting the structural degradation of PBAs.⁴⁷

High-entropy materials (HEMs) have emerged as a promising approach to improve the electrochemical properties of PBAs.⁴⁹ Pioneering work by Ma et al. involved the synthesis of a high-entropy PBAs, $\text{Na}_x(\text{FeMnNiCuCo})[\text{Fe}(\text{CN})_6]$, where five distinct metal species were incorporated in equal molar ratios at the nitrogen-coordinated sites.⁵⁰ This HE-PBAs, engineered through entropy maximization, displays a near-zero volume change during sodium ion intercalation/deintercalation. Liu et al. developed a HEPBA with the composition $\text{Na}_{1.3}\text{Fe}_{0.45}\text{Mg}_{0.13}\text{Ni}_{0.14}\text{Cu}_{0.14}\text{Zn}_{0.14}[\text{Fe}(\text{CN})_6]_{0.94} \cdot 1.9\text{H}_2\text{O}$ by introducing inactive metals (Cu, Ni, Zn, and Mg) into the M sites.⁴⁹ The material retains a stable cubic structure throughout charge/discharge cycles, effectively suppressing lattice distortion. This HEPBA delivers an initial capacity of 107.9 mAh g^{-1} at 0.5C , retaining 81.5 mAh g^{-1} after 500 cycles (Fig. 4d-f). Remarkably, it also shows outstanding long-term durability, sustaining 2000 cycles at 1C with minimal degradation.

Structure designing

PBAs cathodes suffer from significant mechanical degradation during cycling due to phase-transition-induced stress heterogeneity and volume variations during Na^+ insertion/extraction, leading to cracking and poor stability. To address these challenges, core-shell architectures have been developed as an effective solution, where the shell layer provides elastic buffering to accommodate volume changes while minimizing core stress, enhances conductivity through dopant incorporation and heterointerface formation, and reinforces structural integrity.⁵¹⁻⁵⁴ An example is the MnHCF@Fe/MnHCF composite synthesized via an acid-assisted method, which forms a Mn-doped FeHCF shell on MnHCF cores, demonstrating 95.5% capacity retention after 400 cycles at 1 A g^{-1} and excellent rate capability (134.2 mAh g^{-1} at 10 mA g^{-1}) (Fig. 5a).⁵¹ PW@PB and CoHCF@FeHCF also showed superior electrochemical performance.⁵³⁻⁵⁴ Yuan et al. reported a triple-layer FeHCF@MnHCF@FeHCF structure where the inner and outer FeHCF shells work synergistically to suppress Jahn-Teller distortion in the MnHCF core while preventing Mn dissolution, achieving 140.2 mAh g^{-1} at 10 mA g^{-1} with outstanding cycling stability (Fig. 5b).⁵²

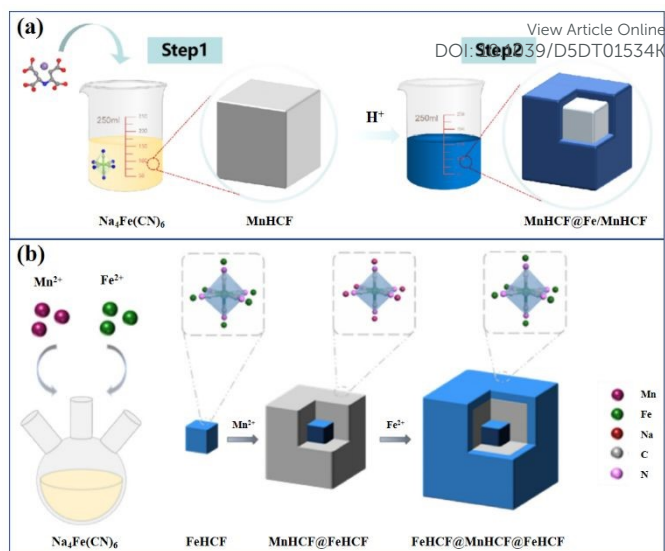


Fig. 5 Schematic illustration of the synthesis process of MnHCF@Fe/MnHCF (a). Reproduced with permission. Copyright 2025, Elsevier.⁵¹ and FeHCF@MnHCF@FeHCF (b). Reproduced with permission. Copyright 2025, Elsevier.⁵²

Conductive polymer, such as polypyrrole (PPy),⁵³ polyaniline (PANI)⁵⁴ and poly-3,4-ethylenedioxythiophene (PEDOT),⁵⁵ applied to PBAs coatings can also significantly improve the interfacial charge transfer kinetics and mitigate cathode-electrolyte side reactions. Their intrinsic chemical resistance and mechanical flexibility maintain structural integrity of PBAs during prolonged electrochemical cycling. For instance, Yuan et al.⁵⁶ employed a vapor-phase molecular self-assembly technique to fabricate NaFeHCF/PPy. The incorporation of a PPy protective layer not only improves the electronic conductivity, but also effectively mitigates the dissolution of Fe-ions during cycling. The NaFeHCF@PPy exhibited a remarkably enhanced cycling performance, with capacity retentions of 85.6% and 69.1% over 500 and 1000 cycles, respectively.

Some inorganic metal compounds also possess excellent chemical stability and have promising potential as coating layers for PBAs.⁵⁷⁻⁵⁹ Xu et al. constructed a magical Co_xB skin on the surface of MnHCF.⁵⁹ Benefited from the complete coverage and the buffer effect of Co_xB layer, the modified MnHCF cathode exhibits suppressed Mn dissolution and reduced intergranular cracks inside particles, thereby demonstrating thousands-cycle level cycling lifespan.

Scalable synthesis

Scalable synthesis of PBAs is critically necessary to unlock their full potential for sodium-ion batteries. Significant progress has been made through batch precipitation methods: Wang et al. successfully prepared rhombohedral $\text{Na}_{2-x}\text{FeFe}(\text{CN})_6$ on a 5 kg scale using a 100 L reactor, achieving stable cycling performance over a thousand cycles (Fig. 6a-b).⁶² Xu et al. achieved kilogram-grade synthesis of MnNi-PB and MnFeNi-PB using a 100 L reactor through coprecipitation method, both of the Mn-based PBAs demonstrated good electrochemical performance (Fig. 6c-d).^{63, 64} Complementing these batch approaches, Wang et al. developed a continuous segmented flow microfluidic strategy

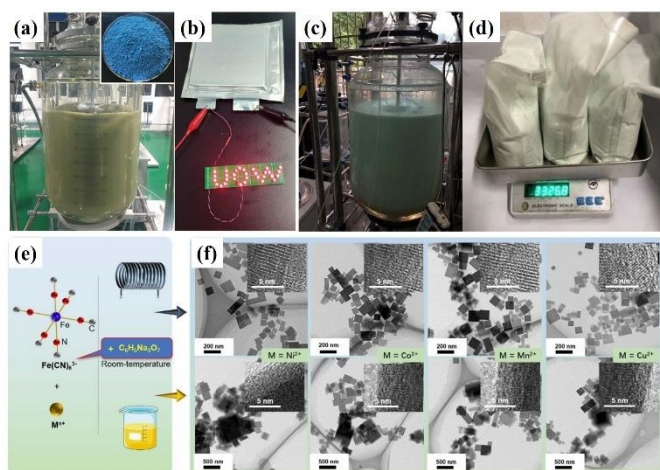


Fig. 6 Digital image of synthesis of Prussian white $\text{Na}_{2-x}\text{Fe}(\text{CN})_6$ in 100 L reactor and powder of final product (a), digital image of pouch full cell connected with red LED lights (b). Reproduced with permission. Copyright 2020, Springer Nature.⁶² Synthesis of $\text{Mn}_{0.5}\text{Ni}_{0.5-0.5}$ with a 100 L reactor (c), Kilogram-grade $\text{Mn}_{0.5}\text{Ni}_{0.5-0.5}$ sample after one preparation (d). Reproduced with permission. Copyright 2022, American Chemical Society.⁶⁴ Schematic illustration of microfluidic segmented flow synthesis and bulk solution synthesis of Ni-/Co-/Mn-/Cu-based PBAs (e), representative TEM images of different PBAs as noted in microfluidic reactor (up) and conventional bath reactor (down) (f). Reproduced with permission. Copyright 2024, Wiley.⁶⁵

enabling rapid synthesis (within minutes) of highly dispersed and crystalline ZnHCF nanocubes.⁶⁵ This microfluidic process can be extended to synthesize PBAs like NiHCF, CoHCF, MnHCF, and CuHCF (Fig. 6e-f).

Scalable synthesis of PBAs—from kilogram-scale batch precipitation to continuous microfluidic nanocube production—enables high-yield, low-defect cathodes while maintaining exceptional cycling stability and crystallinity, unlocking their commercial potential for sodium-ion batteries.

Summary and Outlook

PBAs have emerged as highly promising cathode materials for SIBs, offering advantages such as a robust 3D open framework, high theoretical capacity, and cost-effective synthesis. The electrochemical performance of PBAs is fundamentally governed by their unique crystal structure and sodium storage mechanisms. Critical challenges include $[\text{Fe}(\text{CN})_6]$ vacancies, crystal water content, and irreversible phase transitions during cycling, all of which significantly impact their performance and safety. This review systematically examines recent progress in optimizing PBA-based cathodes through advanced synthesis methods, post-treatment, composition engineering, structure designing and scalable synthesis. Innovative approaches such as hydrothermal methods with buffer systems, solvent engineering, and mechanochemical synthesis have enabled precise control over crystallinity, defect concentration, and water content. Post-treatment techniques including optimized washing procedures and controlled thermal dehydration have further improved the performance. Composition engineering, especially the development of high-entropy PBAs with multiple transition metals, have demonstrated remarkable improvements in structural stability and electrochemical

properties. The core-shell structural effectively mitigate mechanical degradation in PBAs cathodes by providing elastic buffering for volume changes.

The development of PBAs as high-performance cathodes for sodium-ion batteries requires focused efforts on several key fronts. First, advanced synthesis and post-treatment methods must be developed to further minimize $[\text{Fe}(\text{CN})_6]$ vacancies and crystal water while maintaining structural integrity, potentially through novel crystallization techniques and optimized dehydration processes. Second, innovative compositional engineering strategies, including high-entropy designs and machine learning-guided doping, should be pursued to stabilize the framework against phase transitions and Jahn-Teller distortions. Third, scalable and environmentally friendly manufacturing processes need to be established to enable cost-effective mass production, with particular attention to continuous-flow reactors and mechanochemical approaches. While significant progress has been made, realizing the full potential of PBAs will require continued interdisciplinary collaboration to bridge the gap between laboratory-scale innovation and commercial viability, ultimately positioning them as a sustainable and competitive alternative to lithium-ion battery cathodes for grid-scale energy storage applications.

Author contributions

Shumin Sun: conceptualization, writing – original draft, writing – review & editing, project administration, and funding acquisition; Xingqi Jiang: writing – original draft, and writing – review & editing; Ziyu Wang: writing – review & editing; Haibo Lei: writing – review & editing; Yongqin Zhai: writing – review & editing; Peiyuan Wang: conceptualization, writing – review & editing, visualization, and funding acquisition. All authors read and contributed to the critical review of the manuscript for intellectual content and approved the submission for publication.

Conflicts of interest

There are no conflicts to declare.

Data availability

No primary research results, software or code have been included and no new data were generated or analysed as part of this review. here are no original data associated with this manuscript.

Acknowledgements

This work is supported by the National Natural Science Foundation of China-Henan Joint Fund (U23A20579), Natural Science Foundation of Henan Province (242300421258), and Henan Provincial Science and Technology Research Project (252102240010).

Notes and references

- 1 K. Shahzadi, X. Zhao, Q. Liu, W. He, D. Mu, Y. Li, L. Li, R. Chen and F. Wu, *Adv. Sustain. Syst.*, 2025, **9**, 2401045.
- 2 Q. Wang, C. Zhao and M. Wagemaker, *Acc. Chem. Res.*, 2025, **58**, 1742.
- 3 J. Hu, X. Li, Q. Liang, L. Xu, C. Ding, Y. Liu and Y. Gao, *Nano-Micro Lett.*, 2025, **17**, 33.
- 4 T. Yuan, Y. Chen, X. Gao, R. Xu, Z. Zhang, X. Chen and L. Cui, *Small Methods*, 2024, **8**, 2301372.
- 5 G. Goel, M. Sharma and S. K. Tripathi, *J. Energy Storage*, 2025, **126**, 116995.
- 6 F. Wu, L. Zhao, L. Wang, L. Xie, Q. Han, X. Qiu, X. Cao and L. Zhu, *Nano Energy*, 2025, **134**, 110534.
- 7 R. Berthelot, D. Carlier and C. Delmas, *Nat. Mater.*, 2011, **10**, 74.
- 8 J. A. K. Satrughna, A. R. Kanwade, S. M. Rajore, M. K. Tiwari, Y. Ito, A. Ogura, H. Lee, Y. Ohshita, and P. M. Shirage, *Electrochim. Acta*, 2024, **507**, 145201.
- 9 N. Yabuuchi, H. Yoshida and S. Komaba, *Electrochemistry*, 2012, **80**, 716.
- 10 E. Lee, D. E. Brown, E. E. Alp, Y. Ren, J. Lu, J.-J. Woo, and C. S. Johnson, *Chem. Mater.*, 2015, **27**, 6755.
- 11 X. H. Ma, H. L. Chen and G. Ceder, *J. Electrochem. Soc.*, 2011, **158**, A1307.
- 12 K. Kubota, I. Ikeuchi, T. Nakayama, C. Takei, N. Yabuuchi, H. Shiiba, M. Nakayama, and S. Komaba, *J. Phys. Chem. C*, 2015, **119**, 166.
- 13 H. Wang, X.-Z. Liao, Y. Yang, X. Yan, Y.-S. He and Z.-F. Ma, *J. Electrochem. Soc.*, 2016, **163**, A565.
- 14 Y. Xie, H. Wang, G. Xu, J. Wang, H. Sheng, Z. Chen, Y. Ren, C.-J. Sun, J. Wen, J. Wang, D. J. Miller, J. Lu, K. Amine, and Z.-F. Ma, *Adv. Energy Mater.*, 2016, **6**, 1601306.
- 15 Y. Lu, L. Wang, J. Cheng and J. B. Goodenough, *Chem. Commun.*, 2012, **48**, 6544.
- 16 J. Song, L. Wang, Y. Lu, J. Liu, B. Guo, P. Xiao, J.-J. Lee, X.-Q. Yang, G. Henkelman and J. B. Goodenough, *J. Am. Chem. Soc.*, 2015, **137**, 2658.
- 17 Y. Huang, W. Mu, J. Meng, X. Bi, X. Lei and S. Luo, *Chem. Eng. J.*, 2024, **499**, 156410.
- 18 H. Yao, Y. Gao, X. Lin, H. Zhang, L. Li and S. Chou, *Adv. Energy Mater.*, 2024, **14**, 2401984.
- 19 Y. Xiao, J. Xiao, H. Zhao, J. Li, G. Zhang, D. Zhang, X. Guo, H. Gao, Y. Wang, J. Chen, G. Wang and H. Liu, *Small*, 2024, **20**, 2401957.
- 20 P. Hong, C. Xu, C. Yan, Y. Dong, H. Zhao and Y. Lei, *Acs Energy Lett.*, 2025, **10**, 750.
- 21 Y. Liu, Y. Qiao, W. Zhang, Z. Li, X. Ji, L. Miao, L. Yuan, X. Hu and Y. Huang, *Nano Energy*, 2015, **12**, 386.
- 22 X. Wu, C. Wu, C. Wei, L. Hu, J. Qian, Y. Cao, X. Ai, J. Wang and H. Yang, *Acs Appl. Mater. Interfaces*, 2016, **8**, 5393.
- 23 Y. You, X.-L. Wu, Y.-X. Yin and Y.-G. Guo, *Energy Environ. Sci.*, 2014, **7**, 1643.
- 24 Y. You, X. Yu, Y. Yin, K.-W. Nam and Y.-G. Guo, *Nano Res.*, 2014, **8**, 117.
- 25 W. Gong, R. Zeng, S. Su, M. Wan, Z. Rao, L. Xue and W. Zhang, *J. Nanopart. Res.*, 2019, **21**, 274.
- 26 W. Wang, Y. Gang, J. Peng, Z. Hu, Z. Yan, W. Lai, Y. Zhu, D. Appadoo, M. Ye, Y. Cao, Q.-F. Gu, H.-K. Liu, S.-X. Dou and S.-L. Chou, *Adv. Funct. Mater.*, 2022, **32**, 2111727.
- 27 P. Wang, D. Zhu, Y. Li, Y. Liu, W. Zhao, Y. Zhang, S. Sun and S. Fang, *Chem. Commun.*, 2024, **60**, 1603.
- 28 Y. Tang, L. Wang, J. Hu, M. Chen, M. Zhou, K. Wang and K. Jiang, *Adv. Energy Mater.*, 2024, **14**, 2303015.
- 29 W. Geng, Z. Zhang, Z. Yang, H. Tang and G. He, *Chem. Commun.*, 2022, **58**, 4472.
- 30 X. Xu, S. Zhu, C. Yang, Y. Wang, Z. Wu, J. Zheng, J. Wu and Y. Gao, *J. Mater. Chem. A*, 2025, **13**, 11848.
- 31 Z. Li, S. Zhong, B. Zhou, D. Chen, Z. Qiu, R. Zhang, R. Zheng, C. Zhao and J. Zhou, *Materials*, 2025, **18**, 1455.
- 32 J. Peng, Y. Gao, H. Zhang, Z. Liu, W. Zhang, L. Li, Y. Qiao, W. Yang, J. Wang, S. Dou and S. Chou, *Angew. Chem. Int. Ed.*, 2022, **61**, 2205867.
- 33 Y. Gao, X. Zhang, H. Zhang, J. Peng, W. Hua, Y. Xiao, X. H. Liu, L. Li, Y. Qiao, J. Z. Wang, C. Zhang and S. Chou, *Adv. Mater.*, 2025, **37**, 2409782.
- 34 P. Wang, Y. Li, D. Zhu, F. Gong, S. Fang, Y. Zhang and S. Sun, *Dalton Trans.*, 2022, **51**, 9622.
- 35 F. M. Maddar, D. Walker, T. W. Chamberlain, J. Compton, A. S. Menon, M. Copley and I. Hasa, *J. Mater. Chem. A*, 2023, **11**, 15778.
- 36 L. Ge, Y. Song, P. Niu, B. Li, L. Zhou, W. Feng, C. Ma, X. Li, D. Kong, Z. Yan, Q. Xue, Y. Cui and W. Xing, *Acs Nano*, 2024, **18**, 3542.
- 37 X. Wang, M. Zhao, W. Du, C. Zhang, W. Li, C. Yang and Y. Liu, *Chem. Eng. J.*, 2025, **508**, 160997.
- 38 Y. Du, X. Wang, Y. Zhu, H. Zhang, M. Wei, H. Zhang, H. Ma, B. Wang, Y. Cui, J. Ji, Y. He, K. Song, N. A. A. Ghany, M. M. G. Fouda and M. Xue, *Chem. Eng. J.*, 2025, **510**, 161687.
- 39 M. Wan, R. Zeng, J. Meng, Z. Cheng, W. Chen, J. Peng, W. Zhang, and Y. Huang, *Nano-Micro Lett.*, 2022, **14**, 9.
- 40 J. Li, L. Liu, Y. Gao, X. Zhou, M. Fang, J. Guo, X. Zhou, B. Zhang, C. Jia, B. B. Xu and Y. Jiang, *EcoMat*, 2025, **7**, e70000.
- 41 Y. Gao, X. Wu, L. Wang, Y. Zhu, G. Sun, Y. Tang, M. Yan and Y. Jiang, *Adv. Funct. Mater.*, 2024, **34**, 2314860.
- 42 L. Xu, Y. Liu, M. Chen, W. Wu, S. Qiu, H. Wu, M. Zheng, X. Zhang and X. Wu, *Chem. Eng. Sci.*, 2025, **302**, 120848.
- 43 T. Yimtrakarn, Y.-A. Lo, J. Kongcharoenkitkul, J.-C. Lee and W. Kaveevivitchai, *Chem. Asian J.*, 2024, **19**, e202301145.
- 44 Z. Zhou, Y. Dong, Y. Ma, H. Zhang, F. Meng, Y. Ma and Y. Wu, *Susmat*, 2025, **5**, e265.
- 45 L. Li, J. Shen, H. Yang, Z. Li, Z. Chen, Y. Yao, W. Li, X. Wu, X. Rui and Y. Yu, *Adv. Energy Mater.*, 2024, **14**, 2401729.
- 46 H. Zhang, J. Peng, L. Li, Y. Zhao, Y. Gao, J. Wang, Y. Cao, S. Dou and S. Chou, *Adv. Funct. Mater.*, 2022, **33**, 2210725.
- 47 Y. Wang, N. Jiang, J. Liu, S. Sun, X. Wang, J. Yang, C. Yang and Y. Liu, *Adv. Funct. Mater.*, 2024, **34**, 2406809.
- 48 B. He, M. Huang, Y. Yu, J. Meng, H. Zhang, J. Li and X. Wang, *Chem. Eur. J.*, 2025, **31**, 2500880.
- 49 S. Liu, H. Yu, Y. Zhao, J. Sun, Y. He, D. Zhu, Z. Song, S. Xu, R. Sun, Y. Yang, S. Tong, R. Zhang, G. Chen and Q. Li, *Small*, 2025, 2504893.
- 50 Y. Ma, Y. Ma, S. L. Dreyer, Q. Wang, K. Wang, D. Goonetilleke, A. Omar, D. Mikhailova, H. Hahn, B. Breitung and T. Brezesinski, *Adv. Mater.*, 2021, **33**, 2101342.
- 51 K. Wang, M. Yang, Q. Liu, S. Cao, Y. Wang, T. Hu and Z. Peng, *J. Colloid Interf. Sci.*, 2025, **678**, 346.
- 52 H. Yuan, Y. Meng, B. Li and F. Zhu, *J. Energy Storage*, 2025, **110**, 115307.
- 53 W.-J. Li, S.-L. Chou, J.-Z. Wang, J.-L. Wang, Q.-F. Gu, H.-K. Liu, and S.-X. Dou, *Nano Energy*, 2015, **13**, 200.
- 54 Q. Zhang, L. Fu, J. Luan, X. Huang, Y. Tang, H. Xie, and H. Wang, *J. Power Sources*, 2018, **395**, 305.
- 55 X. Wang, B. Wang, Y. Tang, B. B. Xu, C. Liang, M. Yan, and Y. Jiang, *J. Mater. Chem. A*, 2020, **8**, 3222.
- 56 T. Yuan, X. Fu, Y. Wang, M. Li, S. Xia, Y. Pang, and S. Zheng, *Nano Res.*, 2024, **17**, 4221.
- 57 M. Morant-Giner, R. Sanchis-Gual, J. Romero, A. Alberola, L. García-Cruz, S. Agouram, M. Galbiati, N. M. Padial, J. C. Waerenborgh, C. Martí-Gastaldo, S. Tatay, A. Forment-Aliaga, and E. Coronado, *Adv. Funct. Mater.*, 2018, **28**, 1706125.
- 58 Y. Qiao, G. Wei, J. Cui, M. Zhang, X. Cheng, D. He, S. Li, and Y. Liu, *Chem. Commun.*, 2019, **55**, 549-552.
- 59 C. Xu, Y. Ma, J. Zhao, P. Zhang, Z. Chen, C. Yang, H. Liu, and Y.-S. Hu, *Angew. Chem. Int. Ed.*, 2023, **135**, e202217761.
- 60 Z. T. Pan, Z. H. He, J. F. Hou and L. B. Kong, *Small*, 2023, **19**, 2302788.

- 61 Y. Wang, Q. Zheng, Y. Pang, Y. Zhang, T. Yuan and S. Zheng, *J. Energy Storage*, 2025, **111**, 115424.
- 62 W. Wang, Y. Gang, Z. Hu, Z. Yan, W. Li, Y. Li, Q.-F. Gu, Z. Wang, S.-L. Chou, H.-K. Liu and S.-X. Dou, *Nat. Commun.*, 2020, **11**, 980.
- 63 Z. Xu, Y. Sun, J. Xie, Y. Nie, X. Xu, J. Tu, C. Shen, Y. Jin, Y. Li, Y. Lu, A. Zhou, F. Chen, T. Zhu and X. Zhao, *Mater. Today Sustain.*, 2022, **18**, 100113.
- 64 Z. Xu, Y. Sun, J. Xie, Y. Nie, X. Xu, J. Tu, J. Zhang, L. Qiu, T. Zhu and X. Zhao, *ACS Sustainable Chem. Eng.*, 2022, **10**, 13277.
- 65 M. Wang, J. Ma, K. Lu, S. Lu and H. Zhang, *ChemSusChem*, 2024, **17**, e202400552.

View Article Online
DOI: 10.1039/D5DT01534K

- No primary research results, software or code have been included and no new data were generated or analysed as part of this review.

[View Article Online](#)
DOI: 10.1039/D5DT01534K